nature ecology & evolution

SUPPLEMENTARY INFORMATION

https://doi.org/10.1038/s41559-020-1241-3

In the format provided by the authors and unedited.

The delayed and geographically heterogeneous diversification of flowering plant families

Santiago Ramírez-Barahona[1]✉, Hervé Sauquet[2,3,4] and Susana Magallón[1]

[1]Departamento de Botánica, Instituto de Biología, Universidad Nacional Autónoma de México, Mexico City, Mexico. [2]National Herbarium of New South Wales, Royal Botanic Gardens and Domain Trust, Sydney, New South Wales, Australia. [3]Evolution and Ecology Research Centre, School of Biological, Earth and Environmental Sciences, University of New South Wales, Sydney, New South Wales, Australia. [4]Université Paris-Saclay, CNRS, AgroParisTech, Ecologie Systématique et Evolution, Orsay, France. ✉e-mail: santiago.ramirez@ib.unam.mx

The delayed and geographically heterogenous diversification of flowering plant families

Santiago Ramírez-Barahona[1], Hervé Sauquet[2-4], Susana Magallón[1]

[1] Departamento de Botánica, Instituto de Biología, Universidad Nacional Autónoma de México, Circuito Exterior s/n, Ciudad de México, 04510, Mexico; [2] National Herbarium of New South Wales (NSW), Royal Botanic Gardens and Domain Trust, Sydney, Australia; [3] Evolution and Ecology Research Centre, School of Biological, Earth and Environmental Sciences, University of New South Wales, Sydney, Australia; [4] Ecologie Systématique Evolution, Univ. Paris-Sud, CNRS, AgroParisTech, Université Paris-Saclay, 91400, Orsay, France.

Supplementary Information

- This file contains Supplementary Methods, Supplementary figures 1 to 9, Supplementary tables 1 to 3, and a list of supplementary data files.
- Supplementary data files are available at *Zenodo* with the identifiers doi.org/10.5281/zenodo.3820878 and doi.org/10.5281/zenodo.3828071.
- Data and code citation:
    - Ramírez-Barahona, S., Sauquet, H. & Magallón, S. The delayed and geographically heterogenous diversification of flowering plant families (Version v1.0) [Data set]. *Zenodo* (2020). doi.org/10.5281/zenodo.3820878.
    - Sauquet, H., Ramírez-Barahona, S. & Magallón, S. A revised list of fossil calibrations to constrain molecular dating of angiosperms (Version v1.0) [Data set]. *Zenodo* (2020). doi.org/10.5281/zenodo.3828071.

Supplementary Information

Table of Contents

Supplementary Methods 3

Molecular and taxonomic sampling 3
Phylogenetic analyses 4
Fossils for calibration 7
Maximum age constraints 11
Fossil calibration sets 13
Penalized likelihood dating analyses 13
Bayesian dating analyses 14
Family age estimates across analyses 15
Geographic data processing 16
Spatial patterns of angiosperm diversity 19
Biome analyses 20

Supplementary References 23

Supplementary Table 1 27

Supplementary Table 2 28

Supplementary Table 3 29

Supplementary Figure 1 30

Supplementary Figure 2 31

Supplementary Figure 3 32

Supplementary Figure 4 33

Supplementary Figure 5 34

Supplementary Figure 6 35

Supplementary Figure 7 36

Supplementary Figure 8 37

Supplementary Figure 9 38

List of Supplementary Data files 39

Supplementary Methods

Molecular and taxonomic sampling

Our taxonomic sampling was based on a list of 435 currently recognized families according to the Angiosperm Phylogeny Website[1] (last accessed February 2018), but with four differences: (1) Coldeniaceae and Hoplestigmataceae were segregated from Cordiaceae (Boraginales)[2]; (2) Lennoaceae, although sampled, was here treated as part of Ehretiaceae (Boraginales); (3) Balonophoraceae (Santalales) was segregated into families Balonophoraceae and Mystropetalaceae[3]; and (4) *Afrothismia* was segregated from Thismiaceae (Dioscoreales)[4] and sampled separately.

We reviewed available phylogenetic studies for each family to identify each family's crown node (*i.e.,* the most recent common ancestor of all living members of the family, also corresponding to the deepest split in the family) and selected placeholder species for each of the two branches stemming from that node. When the deepest split (*i.e.*, crown node) of a family was unresolved, multiple taxa were sampled to span all branches involved in the polytomy. After selecting candidate taxa for every family, we obtained nucleotide sequences through direct searches in GenBank. If particular markers were unavailable for the candidate taxa, the missing sequences were sampled from other species within the same genus or subclade. We tried to keep such alignment chimeras to a minimum and ensured that these were composed of species belonging to the same basal branch derived from the crown node (*i.e.*, monophyletic). For families with no published phylogenies we initially retrieved sequences for all species represented in GenBank.

In addition, we decided to sample species-rich families more densely, for four reasons: (1) to give a more balanced representation among families; (2) to allow more effective fossil calibration points; (3) to include all of the recognized subfamilies (or tribes)

for the largest families with stable phylogenetic classifications; and (4) to expand the potential application of our tree to a broad range of macroevolutionary questions. Thus, species-rich families were arbitrarily defined as those with more than 2,000 accepted species (*ca.* 0.6% of the total species diversity). For the 37 families that fell in this criterion, we applied the same selection methodology to sample species representing the deepest split for every subfamily (or major clade) recognized by the Angiosperm Phylogeny Website[1]. We also included one terminal per major infra-family clade for 22 families with 500-2,000 species; if necessary, we extended the sampling for particular families to include all recognized major infra-family clades.

Based on the ML tree topology (see ***Phylogenetic analyses*** below), we downsized the molecular dataset to reduce the overrepresentation of particular families (*e.g.*, those with no published phylogeny) by selecting two taxa representing the deepest split within each family, while maximizing sequence length. The original molecular dataset included 1,869 taxa of angiosperms (extended sample), which was downsized to 1,209 taxa for the final taxonomic sample. In specific cases, we retained additional taxa to achieve more precise fossil calibrations. The list of GenBank accessions for all sequences is presented in **Supplementary Data 8**.

Phylogenetic analyses

Sequences for each molecular marker were aligned using ClustalW v.2.0[5], followed by manual refinement using Geneious v.6 (www.geneious.com). Because of difficulties in homology assessment in *ndhF*, we eliminated highly variable regions consisting of contiguous simple sequence repeats. The concatenated alignment of nucleotide sequences for the seven molecular markers is 11,395 base pairs long. Although the nuclear *5.8S* region only encompasses 164 base pairs, its inclusion provided phylogenetic resolution for parasitic families for which plastid sequences were mostly unavailable. The

average pairwise identity among aligned sequences for all markers was 88% (with a range of 78–95%), with a per-site and a per-taxon missing data of 26% and 33%, respectively (sequence alignment available as **Supplementary Data 7**).

We performed multiple preliminary rounds of ML phylogenetic inference for each molecular marker individually using RAxML v.8[6] with the GTRCAT model and automatic bootstrap replicates. We did not perform these preliminary analyses for the *5.8S* alignment. The resulting per-locus ML trees were used to assess the monophyly of families and identify taxa that occupied an unexpected phylogenetic position with respect to consistently obtained relationships, or with unusually long branches. In turn, we revised the sequence alignments and replaced the problematic sequences for specific taxa using simple BLAST queries.

After the multiple rounds of corrections, we conducted a phylogenetic analysis on the original molecular dataset of 1,869 taxa (extended sample) using RAxML v.8[6] with the GTRCAT model and automatic bootstrap replicates. Substitution parameters were estimated independently for five data partitions: (1) first and second positions of *rbcL* and *atpB*; (2) third position of *rbcL* and *atpB*; (3) *matK*; (4) *ndhF*; and (5) *18S* plus *26S* plus *5.8S*. We included six gymnosperm taxa and specified the fern genus *Ophioglossum* as the outgroup. Initially, we did not implement any topological constraints on the tree inference, but preliminary results led us to use four major topological constraints: (1) the heterotrophic family Apodanthaceae (Cucurbitales) was consistently embedded within monocots, forcing us to constraint the monophyly of Cucurbitales[7]; (2) similarly, the monophyly of Achariaceae (Malpighiales) was forced due to the intrusion of heterotrophic Rafflesiaceae (Malpighiales)[8]; (3) this second restriction resulted in an unconstrained position of Rafflesiaceae within Sapindales, leading us to constrain the monophyly of Malpighiales[8]; and (4) the families Dasypogonaceae and Arecaceae (Arecales) were not

consistently recovered as sister lineages, thus we opted to constrained the monophyly of Arecales (but see ref.[9]).

The final sample of the molecular dataset was used to estimate a ML phylogeny in RAxML v.8[6] with the GTRCAT model, the same partition scheme as above, and 1000 bootstrap replicates (maximum likelihood phylogram available as **Supplementary Data 1**). In addition to the major topological constraints mentioned above (*i.e.,* three orders, one family), the phylogenetic analyses using the 1,209-terminal dataset included constraints on the monophyly of 11 families that were otherwise recovered as monophyletic with the extended sample. In most of these cases, retrieving non-monophyletic families after downsizing the taxonomic sample can be attributed to missing molecular data or to the presence of highly variable sequences for heterotrophic taxa. Similarly, additional monophyletic constraints were applied to 36 subfamilies (tree with topological constraints is available as **Supplementary Data 9**). All ML analyses were performed in the CIPRES Science Gateway portal[10].

Our phylogenetic tree agrees with well-established relationships among major groups[1,11,12]. In general, our new estimated phylogeny (with the tip constraints outlined above) shows Amborellales, Nymphaeales, and Austrobaileyales as successive sister groups to the remainder of angiosperms (mesangiosperms). The latter are formed by two major clades: (i) magnoliids, Chloranthales and monocots; and (ii) Ceratophyllales and eudicots. Overall, the phylogenetic tree includes the stem node for all families and the crown node for 94% of all non-monotypic families. Some deep branches in the phylogeny have low bootstrap support, but shallower relationships (*e.g.*, family-level) show moderate to high bootstrap support (>80). Overall, the tree shows moderate to high bootstrap support for 372 of the families with two or more sampled species. Four orders (*i.e.*, Bruniales, Proteales, Metteniusales, Icacinales) and four families (*i.e.*, Nymphaeaceae,

Dioscoreaceae, Salvadoraceae, Metteniusaceae) were consistently recovered as non-monophyletic.

Fossils for calibration

We compiled an entirely new set of fossil calibrations for this study following principles outlined by refs.[13,14], using the PROTEUS database[15] to organize and extract the information. The final set used here consists of 238 angiosperm fossils (including five angiosperm-like fossil pollen grains assigned to their stem lineage), which we provide here in two forms: a summary table and a full justification document available in **Supplementary Data 2**.

Our main aim was to include the oldest known fossil record of each angiosperm family while maximizing reliability. For this reason, we preferred fossils whose node assignment had been obtained in phylogenetic analysis (*e.g.*, total evidence or molecular backbone analysis) or had been justified by clear apomorphies, and whose absolute age was well constrained (*e.g.,* based on radio-isotopic measures or recently revised stratigraphy). However, unlike several recent studies abiding strictly to the best practices of ref.[13], we also included a number of fossils assigned to the phylogeny based on "intuitive" criteria (*sensu* refs.[14,16]). Our rationale behind this choice is that many valuable and highly informative fossils are consistently ignored in most angiosperm-wide molecular dating analyses, where the total number of fossil calibrations typically ranges from 24 to 62[12,17–22]. While we acknowledge that phylogenetic analysis using morphological and molecular data ultimately should underline the node assignment of all fossil calibrations, morphological datasets at this scale are still scarce or not sufficiently sampled to reach this goal yet. In addition, many published phylogenetic analyses of fossil taxa have inherent limitations[23]. Hence, relaxing this criterion allowed us to explore the impact of a much more comprehensive set of fossil calibrations than ever used, to our knowledge, to

estimate divergence times in angiosperms. This is a similar strategy to the recent fossil calibration sets assembled by refs.[24–26]. Nevertheless, we also conducted molecular dating analyses including only fossils justified by phylogenetic analysis (45 in total, see ***Fossil calibration sets*** below).

To compile this list, we started by revising an updated dataset of over 3,400 fossils, which had been assembled as a starting point for the set of 137 calibrations of ref.[25]. We then selected the oldest reported record of each major clade, family, and subfamily or tribe and systematically screened three recent comprehensive calibration reviews on asterids[26], monocots[24], and magnoliids[27] to include preferentially the fossil taxa accepted by these studies when two or more oldest fossils of similar age were available. We also took into account recent significant discoveries reported in the paleobotanical literature (*e.g.*, refs.[28–30]) and well-justified calibration sets published in recent molecular dating studies of selected families or orders (*e.g.*, refs.[14,31,32]). This initial phase led to a list of 317 potential fossil calibrations. We then reviewed extensively the identity, absolute age, and node assignment of each fossil calibration according to an extended grid of fields (in italics below) set up in PROTEUS and inspired by refs.[13,14]. In the following paragraphs, we summarize this process briefly.

(1) Fossil identity: for each fossil taxon, we tracked and documented the *Reference* in which the original description was provided (as well as the latest re-description of the taxon where appropriate), allowing us to cite the *Specimen numbers* attached to this description (matching best practice #1 of ref.[13]). We decided to exclude from the current set any fossil for which we could not personally access the original description, except for rare cases where we relied on a previous, recent review that explicitly cited specimen numbers[24]. In addition, for each fossil, we specified the *Organs* preserved, and the

Locality, *Formation*, and *Country* in which the oldest record (used to provide an age constraint) has been documented.

(2) Fossil age: each fossil was assigned a "safe absolute minimum age" in millions of years based on either a stratigraphic or radio-isotopic age, documented as the *Absolute age source*. For stratigraphic ages, we always used the upper limit of the oldest stratigraphic age and cite both the *Reference time scale* and *Oldest stratigraphic age* used for this conversion. For most fossils, we used the ICS v2017/02 geologic time scale[33], except for internal (informal) divisions of Upper Cretaceous stages (*e.g.*, "early Cenomanian"), where we relied on the more detailed geologic time scale of ref.[34], following the same approach as ref.[27]. We note that formal boundaries of Upper Cretaceous stages are identical between the two time scales. Similarly, in a few cases, we converted informal geological series divisions of the Cenozoic (*e.g.*, "middle Eocene") into minimum stages (e.g., "Lutetian") and made these choices explicit (*e.g.*, "middle Eocene (Lutetian assumed)"). We acknowledge that such decisions entail a small risk of over-estimating a fossil absolute age but believe the benefit of avoiding systematic under-estimation due to stratigraphic uncertainty justifies this approach. In addition, for each fossil, we provide a *Main reference* for the age and a detailed *Age justification*, often sourced directly from this reference in the form of an explicit quote. The main reference for the age may be the same original publication where the fossil was described, or a more recent revision from either the geochronological or the fossil calibration literature. Collectively, this documentation matches best practices #4 and #5 of ref.[13]. For consistency, we homogenized ages across fossils from the same locality or formation (when sourced from the same deposit). For instance, for all fossils from the Claiborne Formation in the U.S.A., we used a Bartonian stratigraphic age (converted to a safe minimum age of 37.8 Ma), following the justification provided in ref.[14]. Finally, each fossil calibration was given an *Age quality score* on a scale

of 1 to 5, where 5 corresponds to ages revised on the basis of radio-isotopic dates, considered to be the most reliable.

(3) Fossil relationships: each fossil was assigned to either the *Crown or stem* node of an explicit *Clade*. A *Reference* is provided for this assignment, along with a detailed *Node justification*, often sourced directly from this reference in the form of an explicit quote. The main reference for node assignment may be the same original publication where the fossil was described, or (more often in this dataset) a more recent revision from the literature taking into account one or more sources of evidence (*e.g.,* phylogenetic analysis) and current understanding of phylogenetic relationships among extant taxa, typically lacking for many fossil taxa described in the pre-molecular era (*i.e.*, before 1990). Hence, most of the references used here for node justification are recent extensive fossil calibration reviews by ourselves and other authors[24,25,27]. In the few cases of valuable fossils for which only an intuitive assignment based on older literature was available and used as the main reference, we converted presumed affinities into explicit node assignments following two rules: 1) any fossil claimed to share the unique combination of characters of a given family (or other taxon) was assumed to constrain the stem node of this family (or other taxon); 2) any fossil claimed to share all the characters of a given extant genus and named as a fossil species of this genus was assumed to constrain the crown node of the family to which the genus belongs. This approach may be seen as both conservative and optimistic. Excluding such intuitively placed fossils was the main rationale for conducting an additional set of analyses restricted only to the subset of phylogenetically placed fossils (see ***Fossil calibration sets*** below). Particular attention was given to variable circumscription of families (or other taxa) throughout the history of angiosperm classification systems: to the best of our knowledge, we have converted taxa referred to in the literature into currently accepted named clades[1] when assigning each

fossil to an explicit node in our database. Finally, each fossil calibration was given both a *Node assignment score* and a *Reconciliation score* on a scale of 1 to 5, where 5 corresponds to phylogenetic analysis, and to combined morphological and molecular analysis (total evidence or backbone), respectively. These two fields aim specifically at tracking best practices #2 and #3 of ref.[13], while allowing the transparent inclusion of less secure fossils (e.g., based on intuitive assignments by the original authors and without molecular data at hand). Although in this study, we only used the *Node assignment* score as a primary filter to select two calibration sets (see ***Fossil calibration sets*** below), our long-term aim is to allow users of our calibration database to decide themselves the threshold of quality aimed for a particular molecular dating analysis.

Through this process, we excluded a number of doubtful records as well as more recent fossils whose presumed assignment has been challenged by recent phylogenetic analyses by ourselves and other authors (*e.g.*, ref.[35]). Although we aimed primarily at including the oldest fossil record of each angiosperm clade, in a few cases we included more than one age constraint on any given clade, typically for groups with a rich and well documented fossil record. As a result, our final set used here consists of 238 angiosperm fossil age constraints on 203 distinct nodes of our final 1209-taxon tree (a detailed phylogenetic tree with the position of fossil calibrations is available in **Supplementary Data 3**).

Maximum age constraints

To gauge the effect of bracketing the age of crown angiosperms on family divergence times, we used three calibration strategies: *constrained calibration* (CC), *relaxed calibration* (RC), and *unconstrained calibration* (UC). In all three analyses, we used a uniform distribution on the root of the tree (*i.e.*, crown seed plants) based on the 10 and 90% quartiles of the Gamma distribution provided by ref.[36] (368.46–380.49 Mya). For the

CC and RC strategies, the calibration time priors for crown angiosperms were also based on the age distribution provided by ref.[36]. This age distribution was estimated using *PyRate*[36,37], a program that estimates origination, extinction, and preservation rates from fossil occurrence data. In ref.[36] *PyRate* was used to estimate the time of origin of major lineages of vascular plants, including angiosperms. Accordingly, the age for crown angiosperms was best modelled by a Laplace distribution with mean = 144.26 Mya and scale = 4.36. The latter mean age is slightly older than the confidence interval for the age of crown angiosperms estimated by ref.[25] (136–139.35 Mya) using a different fossil-based method[38].

For the CC, we used a uniform prior distribution for crown angiosperms (134.22–154.23 Mya) obtained from the 5.0 and 95.0% quartiles of the Laplace distribution[36]. For the RC, we directly implemented the Laplace distribution as the time prior for crown angiosperms, allowing older ages to be sampled beyond the 95% quartile of the distribution. For the CC and RC, all internal calibrations were given uniform prior distributions using the minimum age constraint set by the fossil and a maximum hard bound of 154.23 Mya.

Alternatively, under the UC we used a uniform distribution for crown angiosperms (134.22–247 Mya), in which the maximum hard bound marks the appearance in the fossil record of the first angiosperm-like pollen grains[39–41]; internal calibrations were given uniform prior distributions with 247 Mya as a maximum hard bound. Although these angiosperm-like pollen grains are potential stem relatives rather than crown-group members of angiosperms[40], the well-sampled nature of the pollen record implies that these fossils provide a plausible, conservative maximum boundary for crown angiosperms.

Fossil calibration sets

To gauge the effect of varying confidence in fossil-based calibrations on family divergence time, we used two different sets of fossils under the three calibration strategies: (1) the *complete* set included all 238 fossils calibrating 203 distinct nodes; (2) the *conservative set* included 45 fossils, calibrating 40 nodes, whose affinities have been assessed using phylogenetic analyses (*e.g.*, total evidence) (**Extended Data figure 1**; **Supplementary Data 2,3**).

Penalized likelihood dating analyses

In order to date the angiosperm phylogeny under each combination of maximum age constraint and fossil set (six analyses), we initially performed penalized likelihood[42] analyses in treePL[43] based on the final maximum likelihood phylogram without the fern outgroup (*i.e.*, sample of 1,209 angiosperms plus 6 outgroups). For the constrained (CC) and unconstrained (UC) calibrations, the age constraints were implemented as described above (see ***Maximum age constraints*** above). Since treePL only accepts strict minimum and maximum age constraints, for the relaxed calibration (RC) strategy the age constraint on crown angiosperms was set to 134.22-368.46 Mya. The lower bound was based on the 5.0% quartile of the Laplace distribution described for angiosperms in ref.[36] and the upper bound was based on the 10% quartile of the Gamma distribution described for seed plants in ref.[36] (see ***Maximum age constraints*** above). The maximum age constraint use in RC is older (368.46 Mya) than the one used for UC (247 Mya). However, this maximum age setting allows for significantly older ages for crown angiosperms, mimicking the fat-tailed Laplace distribution used in the Bayesian dating (see ***Bayesian dating analyses*** below).

Although the fossil-based calibrations used are consistent with each other (*i.e.*, minimum age for a particular node is not older than its ancestor's maximum age), we had to exclude five fossil calibrations due to initialization problems in treePL (Nfos: 352, 125,

197, 337, 215; fossil codes in **Supplementary Data 2**). For each of the six analyses we determined the best optimization parameters and used a smoothing value optimized through RSRCV cross-validation. The resulting dated trees were used as the starting trees for the Bayesian dating analyses (see ***Bayesian dating analyses*** below).

Bayesian dating analyses

For each combination of maximum age constraint and fossil set (six analyses), we ran two independent Markov Chain Monte Carlo (MCMC) runs in BEAST v2.5.1[44] of slightly different lengths for each dating analysis (see below), but under the same conditions, for a total length of *ca.* 250 million generations per analysis. MCMC runs were sampled every 10,000 generations and a burn-in fraction of 20-50%, depending on the analysis, was specified for each run after inspecting the likelihood traces in Tracer v1.7[45]. To minimize computational burden, we partitioned the molecular dataset into one nuclear and one plastid components with a GTR + Γ nucleotide substitution model according to PartitionFinder2[46], used a Birth-Death tree prior, linked the tree and clock model across partitions, and used the penalized likelihood dated phylogeny as the starting tree with a fixed topology (see ***Penalized likelihood dating analyses*** above). The fern outgroup (*Ophioglossum*) was excluded from all dating analyses. We confirmed the influence of the molecular data on the estimated ages by performing all Bayesian analyses for 200 million generations 'without data' in order to sample from the prior.

MCMC chain convergence and mixing were assessed using the '*coda*' package[47] in R[48]; in all the analyses chains converged and most parameters, including the likelihood and the posterior, had an effective sample size > 200. The sampled trees were used to extract a maximum clade credibility tree with node ages defined from the mean node heights in TreeAnnotator[44] (maximum clade credibility trees for all six analyses are available in **Supplementary Data 10**).

Family age estimates across analyses

We retrieved the mean stem and crown age estimates for all orders, families and subfamilies (or tribes), along with the corresponding 95% highest probability density intervals, obtained from the Bayesian analyses under the six combinations of maximum age constraints and fossil sets (family ages are provided in **Supplementary Data 4**). For the Bayesian dating analyses we visualized the distribution of family age with frequency histograms of mean stem and crown age (10 My bins), along with kernel density estimates using the 95% highest probability density intervals for stem and crown ages (Gaussian kernels, bandwidth = 5 My) (**figure 2a** in the main text; **Extended Data figure 4**). We compared family stem and crown age estimates among calibration sets to evaluate the impact of maximum age constraints and fossil sets (**Extended Data figure 4; Supplementary figures 3,4**). Also, we compared the estimated family stem and crown ages across dating methods (*i.e.*, Bayesian, penalized likelihood), showing that penalized likelihood dating gives consistently older age estimates than Bayesian dating (**Supplementary figure 8**).

For the families with crown ages estimates (373 families), family phylogenetic fuses were estimated as the difference between the mean stem and crown ages obtained from the Bayesian analyses under the six combinations of maximum age constraints and fossil sets. We classified families according to the length of the estimated fuse time (short, intermediate, long) by ranking each of the 373 families according to the length of their phylogenetic fuse. Each of the three fuse categories encompasses one third of all families: short (124 families), intermediate (125) and long (124) (**Extended Data figure 2**). We then visualized the distribution of the three fuse categories across the angiosperm phylogeny and estimated the sum of species richness for families within each category.

Geographic data processing

Occurrence data for flowering plants were retrieved from the Global Biodiversity Information Facility by querying all records under 'Magnoliopsida' and 'Liliopsida' that were associated with herbarium specimens (GBIF.org accessed 12th June 2019; GBIF Occurrence Download https://doi.org/10.15468/dl.iftsjs). This dataset consists of approximately 61.8 million occurrence records. From this dataset, we first discarded all records without species identification and then used the *python* script in ref.[49] to eliminate records with imprecise geographic coordinates and those potentially associated with biodiversity institutions. This allowed us to flag around 36.7 million potentially erroneous records. Subsequently, we implemented a series of taxonomic and geographic filters on the remaining occurrence records (*ca.* 25.1 million) to eliminate erroneous or doubtful records, as detailed below. All subsequent processing was conducted in R[48].

We updated family and species names through cross-validation against a list of accepted species names and synonyms available in The Plant List[50] and a list of accepted family names and synonyms available in the Angiosperm Phylogeny Website[1]. The list of names from The Plant List[50], including accepted names and synonyms, contains 951,140 recorded species names[50] and the list of names from the Angiosperm Phylogeny Website[1] contains 1,545 family names. After querying all species in the occurrence data against the lists of species names, we identified 21,668 species that were absent from The Plant List, some of which appear to be clear spelling variants (*e.g.*, *Agave nuusaviorum* = *Agave nussaviorum*, *Epidendrum dukei* = *Epidendrum duckei*). To identify possible spelling variants of accepted names we used the Jaro-Winkler similarity measure as implemented in the *RecordLinkage* package in R[48]. Briefly, this index measures the edit distance between two words, including transpositions, while taking into account the length of the two words, giving values between 0 (no shared letters between words) and 1 (identical

words). For each of the 21,668 suspect names in the occurrence dataset, we computed the Jaro-Winkler similarity to every species name recorded in The Plant List. We identified corresponding valid names with a conservative acceptance threshold of complete similarity for the generic name and a 0.94 similarity for the species epithet. This threshold allows for a few character mismatches between the suspect name and the accepted name. Using this name-matching procedure, we identified 5,107 species names which are very likely spelling variants of accepted names.

We performed additional nomenclatural changes to specific family names *(e.g*., Boraginaceae *sensu* APG IV[11]) in order to obtain a final occurrence database that conforms with the classification herein adopted. For these families, we queried the database for accepted names and synonyms of recognized genera listed in the APWeb[1] and performed the corresponding changes to family names. We obtained a final list of 248,606 accepted species for the 435 accepted families corresponding to the ones used in phylogenetic estimation (see ***Molecular and taxonomic sampling*** above).

For each accepted species, we applied geographical filters using the *CoordinateCleaner* package[51] in R[48] to flag records meeting at least one of the following conditions: (1) equal latitude and longitude; (2) zero latitude and longitude; (3) coordinates falling within a 0.05º radius (~ 5 km^2) of a country's political centroid; (4) coordinates falling within a 0.05º radius (~ 5 km^2) of a country's capital; and (5) coordinates falling within a 0.002º radius (~ 0.2 km^2) of biodiversity institutions. Duplicate records for each species (*i.e.,* identical geographic coordinates) were identified and flagged. Occurrences in the open ocean were flagged as suspect by using a buffered landmass reference available in the *CoordinateCleaner* package[51] in R[48]. This reference landmass is buffered by one degree from the coastline to ensure that coast and marshland species are not flagged as invalid occurrence records. In addition, for each individual species we estimated the

pairwise geographic distances between all of the species' records and defined putatively outlying geographic occurrences as those with a minimum pair-wise distance to all other records of the same species greater than 500 km. These records are single species occurrences isolated from the rest of the known species distribution, which may represent species misidentifications or non-native populations. Finally, we used the Global Naturalized and Alien Flora database[52] to flag geographic occurrences for species classified as naturalized in different regions across the globe. This database provides a list of known (or suspect) alien and naturalized species reported for distinct geographic units (*e.g.*, countries, provinces) throughout the globe.

Out of the initial records (*ca.* 61.8 million), we detected around 36.7 million records with imprecise geographic coordinates, flagged around 7.6 million occurrence records as possible geographical outliers and identified around 1.1 million records as possible non-native occurrences. Thus, the final geographic occurrence data comprised approximately 16.4 million high-quality occurrence records for angiosperm species on a global scale, representing less than a third (26.5%) of the raw occurrence records obtained from GBIF (**Supplementary figure 9**).

Despite the global extent of the occurrence database, there are still some regions that are poorly represented in GBIF. This may produce biases in the spatial patterns of diversity observed across the globe, especially those concerning statistical analyses testing for differences across latitude or between biomes (see ***Spatial patterns of angiosperm diversity*** below). Thus, we performed all analyses excluding grid-cells with less than five reported species, which significantly reduced the number of suspiciously species-poor grid cells observed across the globe, but without affecting the observed geographic patterns.

Spatial patterns of angiosperm diversity

We used the final occurrence database (*ca.* 16.4 million) to construct a global presence-absence matrix of angiosperm species using a grid of 2×2º cells. Basically, a presence-absence matrix corresponds to the distribution of taxa (columns) across a set of geographic units (rows), where an element of the matrix $\lfloor j, i \rfloor$ reflects the presence (1) or absence (0) of taxon *i* (*i*=1,….,*n*) in geographic unit *j* (*j*=1,….*m*). Thus, richness is simply estimated by summing along rows of the matrix. We generated a binary presence-absence matrix of families and transformed into a matrix depicting species richness across the globe. For this, we multiplied every occurrence of family *i* by the number of species recorded for the corresponding family in each grid-cell *j*. Interestingly, family richness is significantly correlated with total species richness as shown by a linear regression on a logarithmic scale (β = 0.64, $F_{(1,4621)}$ = 123940, *p-value* < 0.001, R_2 = 0.96). The spatial patterns of family richness are robust to the taxonomic delimitation of families, as evidenced by the recovery of virtually identical diversity patterns to those obtained by ref.[53] using the APG III system of classification[54].

The observed spatial patterns of mean family age were compared against spatial null expectations on the distribution of family ages. This allowed us to identify regions in space with older or younger mean family ages than expected by chance alone. For this, we constructed two null spatial models to test the spatial pattern that differ in the way the presence-absence matrix was randomized[55]: (1) the NULL 1 randomly shuffles occurrences within sites (*i.e.*, per-row shuffling); and (ii) NULL 2 randomly shuffles occurrences within families (*i.e.*, per-column shuffling). The influence of site richness and family prevalence on the observed patterns are discarded by rejecting NULL 1 or NULL 2, respectively. For each grid-cell, we estimated the standardized effect sizes for the mean family age under the null models (MAF_j^{NULL}), which also were used to test the geographic

patterns of phylogenetic diversity. We documented and compared the geographic patterns of mean age of families (crown and stem), mean phylogenetic fuse of families and mean phylogenetic diversity (PSV) across the three dating analyses using the complete set of fossils. The standardized effect sized showed that the observed patterns are robust across all dating analyses (**Supplementary figures 1,5–7)**. All the statistical and spatial analyses were conducted in R[48].

Globally, mean family crown age showed deviations from the geographic pattern under NULL 1, but not under NULL2. The observed positive standardized effect sizes for mean crown age under NULL 1 suggests that the influence of species richness on the geographic patterns of family crown age is negligible. On the contrary, the distribution of standardized effect sizes for mean crown ages under NULL 2 indicates that family prevalence is relevant for the observed spatial patterns. In the case of mean family stem age, and phylogenetic diversity (as measured by PSV), the distribution of standardized effect sizes under NULL 1 and NULL 2 suggest that both richness and prevalence are important for the observed geographic patterns. However, the two spatial null models are simple random spatial models that do not consider geographic range cohesion.

Biome analyses

To test whether angiosperm age and phylogenetic diversity (as measured by PSV) vary with broad-scale climate conditions, we classified grid-cells according to the distribution of biomes across the globe. We used the latest version of the terrestrial eco-regions and biomes of ref.[56] to avoid issues concerning the arbitrary use of thresholds to define climatic groups of regions. This database classifies terrestrial eco-regions into 14 distinct biomes, which we combined into three ‘super biomes’: arid, temperate, and tropical. The original biomes of ref.[56] were classified as follows:

(1) Temperate: Taiga; Tundra; Tropical Coniferous Forests; Temperate Broadleaf & Mixed Forests; Temperate Coniferous Forests; Temperate Grasslands, Savannas & Shrublands; Montane Grasslands & Shrublands.

(2) Arid: Mediterranean Forests, Woodlands & Scrubs; Deserts & Xeric Shrublands

(3) Tropical: Tropical & Subtropical Moist Broadleaf Forests; Tropical & Subtropical Dry Broadleaf Forests; Tropical & Subtropical Grasslands, Savannas & Shrublands; Mangrove.

Given the climatic variance of the 'Flooded Grasslands' biome, we ignored grid cells falling under this biome, which includes ecologically disparate eco-regions such as the 'Pantanal' eco-region in South America and the 'Tigris-Euphrates alluvial salt marsh' eco-region in Asia.

Our main purpose was to capture major climatic differences across regions. Thus, to test the validity of the 'super biome' classification we performed linear discriminant analyses to test the power of climatic variables to discriminate among the three 'super biome' categories. For this, we used data from the *Climatologies at High resolution for the Earth's Land Surface Areas* database (CHELSA)[57] for eight variables related with temperature and precipitation across the globe (*i.e.,* annual precipitation; precipitation of the driest quarter; precipitation of the wettest quarter; precipitation seasonality; mean annual temperature; mean temperature of the coldest quarter; mean temperature of the warmest quarter; temperature seasonality) and data from the *High-resolution Global Soil-water Balance* database[58] for the Priestley-Taylor alpha coefficient describing the overall aridity stress on vegetation (values approaching 1 indicate that vegetation is not influenced by water stress[58]). The statistical analyses were conducted on a grid of cells with dimensions of 0.25×0.25º. The overall accuracy of climate data to predict the correct

‘super biome’ was 0.85, reflecting the robustness of our ‘super biome’ classification in capturing climatic differences among regions.

To test for significant differences in mean family age and phylogenetic species variability among ‘super biomes’, we employed a linear regression model using super biomes as the predictor variable and mean family age or phylogenetic diversity (as measured by PSV) as the response variables. Significance ($p < 0.01$) of pairwise differences was assessed with a Tukey’s Honest Significant Differences test. The distributions of mean family age and phylogenetic diversity across super biomes were visualized with violin plots, which depict the probability density distribution of a variable across different categories (**Supplementary figure 2**).

Ancestral biomes were then reconstructed on each of the six dated phylogenies implementing the same approach and methods used to reconstruct ancestral floral traits in ref.[59]. Briefly, we first assigned each tip to a named species, choosing the most sampled species across markers for chimeric tips. We then scored the distribution of each sampled species across ‘super biomes’ using the cleaned geographic occurrence data described above across a 2×2º grid of the world. Note that we used a strict exemplar approach for these analyses rather than attempting to capture the full biome occupancy of each family or subclade. We scored a species as present in a particular ‘super biome’ when more than a given percentage of the occurrence records lay within that super biome. Specifically, we used three different thresholds to define presence in a particular biome: (1) majority of occurrences; (2) at least 25% of occurrences; and (3) at least 2.5% of occurrences. Parsimony and maximum likelihood (ML) ancestral state reconstruction (ASR) analyses were conducted on the MCC tree from each of the six BEAST analyses using the *phangorn*[60] and *corHMM*[61] packages in R[48] with custom scripts developed for ref.[59]. For ML analyses, five Markov models were systematically tested, differing in the number of

free transition rate parameters and prior assumptions on the root state (ARD, ARDeq, ER, SYM, SYMeq)[59]. Bayesian reversible-jump Markov Chain Monte Carlo (rjMCMC) ASR analyses were conducted on samples of 1225–1602 trees (depending on calibration scenario) drawn from the posterior of BEAST analyses, using BayesTraits V3[62]. Each rjMCMC analysis was run for 10 million generations, sampling parameters and 15 key nodes every 100 generation, and discarding the first one million generations as burn-in (after checking the stable phase of the chain had been reached).

Our complete results are summarized in **Supplementary Data 5**, and a detailed visual output from our main ML analysis (RC-complete calibration scenario with 25% threshold) is presented in **Supplementary Data 6** (see also **Extended Data figure 5** and **Supplementary table 3**). Maximum likelihood and reversible-jump MCMC analyses reconstruct the Tropical 'super biome' as ancestral in angiosperms, with both a 25% and a 2.5% minimum threshold of occurrence. However, maximum parsimony reconstructed an equivocal ancestral state for angiosperms (Temperate or Tropical) and the maximum likelihood results were sensitive to the calibration scenario and choice of minimum occurrence threshold across our broader range of analyses. For this reason, the reconstruction of the ancestral 'super biome' of angiosperms should be treated with caution.

Supplementary References

1. Stevens, P. F. Angiosperm Phylogeny Website. Version 14. (2001).
2. Luebert, F. *et al.* Familial classification of the Boraginales. *Taxon* **65**, 502–522 (2016).
3. Su, H. J., Hu, J. M., Anderson, F. E., Der, J. P. & Nickrent, D. L. Phylogenetic relationships of Santalales with insights into the origins of holoparasitic Balanophoraceae. *Taxon* **64**, 491–506 (2015).
4. Merckx, V. S. F. T. & Smets, E. F. *Thismia americana*, the 101st Anniversary of a Botanical Mystery. *Int. J. Plant Sci.* **175**, 165–175 (2014).
5. Larkin, M. A. *et al.* Clustal W and Clustal X version 2.0. *Bioinformatics* **23**, 2947–2948 (2007).

6. Stamatakis, A. RAxML version 8: A tool for phylogenetic analysis and post-analysis of large phylogenies. *Bioinformatics* **30**, 1312–1313 (2014).
7. Filipowicz, N. & Renner, S. S. The worldwide holoparasitic Apodanthaceae confidently placed in the Cucurbitales by nuclear and mitochondrial gene trees. *BMC Evol. Biol.* **10**, 219 (2010).
8. Wurdack, K. J. & Davis, C. C. Malpighiales phylogenetics: Gaining ground on one of the most recalcitrant clades in the angiosperm tree of life. *Am. J. Bot.* **96**, 1551–1570 (2009).
9. Givnish, T. J. *et al.* Monocot plastid phylogenomics, timeline, net rates of species diversification, the power of multi-gene analyses, and a functional model for the origin of monocots. *Am. J. Bot.* **105**, 1888–1910 (2018).
10. Miller, M. A., Pfeiffer, W. & Schwartz, T. Creating the CIPRES Science Gateway for inference of large phylogenetic trees. in *Proceedings of the Gateway Computing Environments Workshop (GCE)* 1–8 (2010).
11. APG. An update of the Angiosperm Phylogeny Group classification for the orders and families of flowering plants: APG IV. *Bot. J. Linn. Soc.* **181**, 1–20 (2016).
12. Li, H.-T. *et al.* Origin of angiosperms and the puzzle of the Jurassic gap. *Nat. Plants* **5**, 461–470 (2019).
13. Parham, J. F. *et al.* Best practices for justifying fossil calibrations. *Syst. Biol.* **61**, 346–359 (2012).
14. Sauquet, H. *et al.* Testing the impact of calibration on molecular divergence times using a fossil-rich group: The case of *Nothofagus* (Fagales). *Syst. Biol.* **61**, 289–313 (2012).
15. Sauquet, H. PROTEUS: A database for recording morphological data and fossil calibrations. Version 1.27. (2016).
16. Sauquet, H. A practical guide to molecular dating. *Comptes Rendus Palevol* **12**, 355–367 (2013).
17. Magallón, S. & Castillo, A. Angiosperm diversification through time. *Am. J. Bot.* **96**, 349–365 (2009).
18. Zanne, A. E. *et al.* Three keys to the radiation of angiosperms into freezing environments. *Nature* **506**, 89–92 (2014).
19. Foster, C. S. P. *et al.* Evaluating the impact of genomic data and priors on Bayesian estimates of the angiosperm evolutionary timescale. *Syst. Biol.* **66**, 338–351 (2017).
20. Smith, S. A., Beaulieu, J. M. & Donoghue, M. J. D. An uncorrelated relaxed-clock analysis suggests an earlier origin for flowering plants. *Proc. Natl. Acad. Sci.* **107**, 5897–5902 (2010).
21. Bell, C. D., Soltis, D. E. & Soltis, P. S. The age and diversification of the angiosperms re-revisited. *Am. J. Bot.* **97**, 1296–1303 (2010).
22. Barba-Montoya, J., dos Reis, M., Schneider, H., Donoghue, P. C. J. & Yang, Z. Constraining uncertainty in the timescale of angiosperm evolution and the veracity of a Cretaceous Terrestrial Revolution. *New Phytol.* **218**, 819–834 (2018).
23. Sauquet, H. & Magallón, S. Key questions and challenges in angiosperm macroevolution. *New Phytol.* **219**, 1170–1187 (2018).
24. Iles, W. J. D., Smith, S. Y., Gandolfo, M. A. & Graham, S. W. Monocot fossils suitable for molecular dating analyses. *Bot. J. Linn. Soc.* **178**, 346–374 (2015).
25. Magallón, S., Gómez-Acevedo, S., Sanchéz-Reyes, L. & Hernández-Hernández, T. A metacalibrated time-tree documents the early rise of flowering plant phylogenetic diversity. *New Phytol.* **207**, 437–453 (2015).
26. Martínez-Millán, M. Fossil record and age of the Asteridae. *Bot. Rev.* **76**, 83–135 (2010).

27. Massoni, J., Doyle, J. & Sauquet, H. Fossil calibration of Magnoliidae, an ancient lineage of angiosperms. *Palaeontol. Electron.* **18.1.2FC**, 1–25 (2015).
28. Wilf, P., Carvalho, M. R., Gandolfo, M. A. & Cúneo, N. R. Eocene lantern fruits from Gondwanan Patagonia and the early origins of Solanaceae. *Science (80-.).* **355**, 1–5 (2017).
29. Jud, N. A., Gandolfo, M. A., Iglesias, A. & Wilf, P. Fossil flowers from the early Palaeocene of Patagonia, Argentina, with affinity to Schizomerieae (Cunoniaceae). *Ann. Bot.* **121**, 431–442 (2018).
30. Del Rio, C., Haevermans, T. & De Franceschi, D. First record of an Icacinaceae Miers fossil flower from le Quesnoy (Ypresian, France) amber. *Sci. Rep.* **7**, 1–8 (2017).
31. Zhang, Q., Onstein, R. E., Little, S. A. & Sauquet, H. Estimating divergence times and ancestral breeding systems in Ficus and Moraceae. *Ann. Bot.* **123**, 191–204 (2019).
32. Lavin, M., Herendeen, P. S. & Wojciechowski, M. F. Evolutionary rates analysis of leguminosae implicates a rapid diversification of lineages during the tertiary. *Syst. Biol.* **54**, 575–594 (2005).
33. Cohen, K., Finney, S., Gibbard, P. & Fan, J. The ICS International Chronostratigraphic Chart. *Episodes* **36**, 199–204 (2013).
34. Ogg, J., Hinnov, L. & Huang, C. Cretaceous. in *The Geologic Time Scale.* 793–853 (Elsevier, 2012).
35. Sauquet, H. *et al.* Integrating fossil flowers in angiosperm macroevolutionary analyses [Abstract]. in *Evolution 2019* (2019).
36. Silvestro, D., Cascales-Miñana, B., Bacon, C. D. & Antonelli, A. Revisiting the origin and diversification of vascular plants through a comprehensive Bayesian analysis of the fossil record. *New Phytol.* **207**, 425–436 (2015).
37. Silvestro, D., Schnitzler, J., Liow, L. H., Antonelli, A. & Salamin, N. Bayesian estimation of speciation and extinction from incomplete fossil occurrence data. *Syst. Biol.* **63**, 349–367 (2014).
38. Marshall, C. R. A simple method for bracketing absolute divergence times on molecular phylogenies using multiple fossil calibration points. *Am. Nat.* **171**, 726–742 (2008).
39. Herendeen, P. S., Friis, E. M., Pedersen, K. R. & Crane, P. R. Palaeobotanical redux: Revisiting the age of the angiosperms. *Nat. Plants* **3**, 1–8 (2017).
40. Coiro, M., Doyle, J. A. & Hilton, J. How deep is the conflict between molecular and fossil evidence on the age of angiosperms? *New Phytol.* **223**, 83–99 (2019).
41. Doyle, J. A. Molecular and fossil evidence on the origin of angiosperms. *Annu. Rev. Earth Planet. Sci.* **40**, 301–326 (2012).
42. Sanderson, M. J. Estimating absolute rates of molecular evolution and divergence times: A penalized likelihood approach. *Mol. Biol. Evol.* **19**, 101–109 (2002).
43. Smith, S. A. & O'Meara, B. C. TreePL: Divergence time estimation using penalized likelihood for large phylogenies. *Bioinformatics* **28**, 2689–2690 (2012).
44. Bouckaert, R. *et al.* BEAST 2: A Software Platform for Bayesian Evolutionary Analysis. *PLoS Comput. Biol.* **10**, e1003537 (2014).
45. Rambaut, A., Drummond, A. J., Xie, D., Baele, G. & Suchard, M. A. Posterior summarization in Bayesian phylogenetics using Tracer 1.7. *Syst. Biol.* **67**, 901–904 (2018).
46. Lanfear, R., Frandsen, P. B., Wright, A. M., Senfeld, T. & Calcott, B. Partitionfinder 2: New methods for selecting partitioned models of evolution for molecular and morphological phylogenetic analyses. *Mol. Biol. Evol.* **34**, 772–773 (2017).

47. Plummer, M., Best, N., Cowles, K. & Vines, K. CODA: convergence diagnosis and output analysis for MCMC. *R News* **6**, 7–11 (2006).
48. R Core Team. R: A language and environment for statistical computing. *Vienna R Foudation Stat. Comput.* (2018). doi:10.1007/978-3-540-74686-7
49. Edwards, E. J., de Vos, J. M. & Donoghue, M. J. Doubtful pathways to cold tolerance in plants. *Nature* **521**, E5–E6 (2015).
50. The Plant List. The Plant List. Version 1.1. *Internet* (2013).
51. Zizka, A. *et al.* CoordinateCleaner: Standardized cleaning of occurrence records from biological collection databases. *Methods Ecol. Evol.* **10**, 744–751 (2019).
52. Van Kleunen, M. *et al.* Global exchange and accumulation of non-native plants. *Nature* **525**, 100–103 (2015).
53. Hawkins, B. A., Rodríguez, M. Á. & Weller, S. G. Global angiosperm family richness revisited: Linking ecology and evolution to climate. *J. Biogeogr.* **38**, 1253–1266 (2011).
54. APG. An update of the Angiosperm Phylogeny Group classification for the orders and families of flowering plants: APG III. *Bot. J. Linn. Soc.* **161**, 105–121 (2009).
55. Helmus, M. R., Bland, T. J., Williams, C. K. & Ives, A. R. Phylogenetic measures of biodiversity. *Am. Nat.* **169**, E68–E83 (2007).
56. Olson, D. M. *et al.* Terrestrial ecoregions of the world: a new map of life on Earth. *Bioscience* **51**, 933–938 (2001).
57. Karger, D. N. *et al.* Climatologies at high resolution for the earth's land surface areas. *Sci. Data* **4**, 170122 (2017).
58. Trabucco, A. & Zomer, R. J. Global high-resolution soil-water balance geospatial database. *Published online, available from the CGIAR-CSI GeoPortal* (2010).
59. Sauquet, H. *et al.* The ancestral flower of angiosperms and its early diversification. *Nat. Commun.* **8**, 16047 (2017).
60. Schliep, K. P. phangorn: Phylogenetic analysis in R. *Bioinformatics* **27**, 592–593 (2011).
61. Beaulieu, J. M., O'Meara, B. C. & Donoghue, M. J. Identifying hidden rate changes in the evolution of a binary morphological character: The evolution of plant habit in campanulid angiosperms. *Syst. Biol.* **62**, 725–737 (2013).
62. Pagel, M. & Meade, A. BayesTraits V3.0.1. (2017).
63. Tucker, C. M. *et al.* A guide to phylogenetic metrics for conservation, community ecology and macroecology. *Biol. Rev.* **92**, 698–715 (2017).

Supplementary Table 1

Mean age estimates for flowering plants (angiosperms) and the five key mesangiosperm lineages. Ages in millions of years are based on Bayesian relaxed molecular clock models using six distinct calibration analyses (Supplementary Methods; Supplementary Data 8). CC: constrained calibration; RC: relaxed calibration; UC: unconstrained calibration. Dates are given for the 95% highest posterior density (HPD) estimated for crown and stem ages.

Lineage	Age	Fossil set	CC	RC	UC
Angiospermae	Stem	Complete	368.5–379.8	368.5–379.8	369.1–380.5
		Conservative	368.5–379.7	368.5–379.7	368.5–379.7
	Crown	Complete	153.7–154.2	177.0–218.1	245.0–247.1
		Conservative	153.7–154.2	174.6–205.3	242.6–247.1
Magnoliidae	Stem	Complete	148.3–151.1	155.0–166.1	227.8–238.9
		Conservative	145.5–149.8	153.4–163.1	218.4–235.2
	Crown	Complete	141.5–149.2	145.5–161.3	196.7–236.2
		Conservative	138.4–147.5	143.6–158.5	181.2–227.3
Chloranthales	Stem	Complete	146.4–150.2	152.6–154.2	222.7–235.8
		Conservative	142.8–148.6	150.8–154.3	213.6–231.4
	Crown	Complete	123.0–136.5	123.0–140.2	123.0–189.9
		Conservative	123.0–138.0	123.0–142.0	123.0–188.3
Monocotyledoneae	Stem	Complete	146.4–150.2	152.6–154.2	227.7–235.8
		Conservative	142.8–148.6	150.8–154.3	213.6–231.4
	Crown	Complete	143.7–148.1	149.0–152.9	213.7–227.9
		Conservative	137.3–145.9	144.1–152.3	204.3–222.8
Ceratophyllales	Stem	Complete	148.9–151.2	153.3–154.2	231.5–238.9
		Conservative	145.9–150.0	152.5–154.2	218.7–235.0
	Crown	Complete	3.7–43.7	6.4–44.4	6.4–45.9
		Conservative	2.4–35.3	3.9–35.0	7.5–67.1
Eudicotyledoneae	Stem	Complete	148.9–151.2	153.3–154.2	231.5–238.9
		Conservative	145.9–150.0	152.5–154.2	218.7–235.0
	Crown	Complete	146.7–149.6	150.0–152.7	226.8–234.5
		Conservative	142.8–147.3	147.4–152.5	211.4–229.5

Supplementary Table 2

Mean flowering plant family age estimates per geological period. Mean ages are based on Bayesian relaxed molecular clock models using six distinct calibration analyses. CC: constrained calibration; RC: relaxed calibration; UC: unconstrained calibration. Percentages of families (relative to total) for crown and stem age estimates and percentage of families with phylogenetic fuse times greater than 25 million years are given for each calibration strategy using the complete set and the conservative set of fossil-based calibrations. A total of 435 and 373 families was used to estimate percentages for stem and crown ages, respectively.

	Fossil set	Fuse time	Age	Jurassic	Cretaceous	Cenozoic
CC	Complete	243	Stem	7 (1.6%)	334 (77.5%)	90 (20.8%)
		(55.7 %)	Crown	0 (0.0%)	83 (22.3%)	289 (77.7%)
	Conservative	226	Stem	3 (0.7%)	249 (57.9%)	179 (41.4%)
		(51.8 %)	Crown	0 (0.0%)	34 (9.1%)	338 (90.9%)
RC	Complete	259 (59.4%)	Stem	10 (2.3%)	346 (80.3%)	75 (17.4%)
			Crown	0 (0.0%)	86 (23.1%)	286 (76.9%)
	Conservative	259 (59.4%)	Stem	63 (1.4%)	256 (59.5%)	169 (39.1%)
			Crown	0 (0.0%)	39 (10.5%)	333 (89.5%)
UC	Complete	299	Stem	80 (18.5%)	319 (74.1%)	32 (7.4%)
		(68.6 %)	Crown	5 (1.3%)	159 (42.9%)	208 (55.8%)
	Conservative	299	Stem	48 (11.1%)	314 (72.9%)	69 (16.0%)
		(68.6 %)	Crown	2 (0.5%)	100 (27.1%)	270 (72.4%)

Supplementary Table 3

Ancestral biomes reconstructed for 15 key nodes of the flowering plant phylogeny. Reconstruction was performed using maximum parsimony (MP), maximum likelihood (ML), and reversible-jump Markov Chain Monte Carlo (rjMCMC) as in ref.[59]. These results correspond to the relaxed calibration (RC) phylogeny with the complete set of fossil age constraints and a minimum threshold of 25% for biome occupancy.

Node	MP state(s)	ML state	Prob	rjMCMC state	Prob (mean and 95% HPD)
Angiospermae	Temperate / Tropical	Tropical	0.981	Tropical	0.425 (0.017–0.810)
Mesangiospermae	Temperate / Tropical	Tropical	0.988	Tropical	0.501 (0.000–0.977)
Magnoliidae	Temperate / Tropical	Tropical	0.992	Tropical	0.721 (0.449–0.952)
Monocotyledoneae	Temperate	Tropical	0.987	Tropical	0.390 (0.001–0.763)
Eudicotyledoneae	Temperate	Tropical	0.951	Arid	0.416 (0.097–0.866)
Commelinidae	Tropical	Tropical	0.997	Tropical	0.634 (0.007–0.999)
Pentapetalae	Tropical	Tropical	0.987	Tropical	0.537 (0.000–0.999)
Superasteridae	Tropical	Tropical	0.987	Tropical	0.544 (0.000–0.999)
Asteridae	Tropical	Tropical	0.969	Tropical	0.507 (0.000–0.964)
Lamiidae	Tropical	Tropical	0.981	Tropical	0.577 (0.001–0.997)
Campanulidae	Temperate / Tropical	Tropical	0.857	Temperate	0.538 (0.265–0.957)
Superrosidae	Tropical	Tropical	0.987	Tropical	0.504 (0.000–0.969)
Rosidae	Tropical	Tropical	0.987	Tropical	0.547 (0.000–0.987)
Malvidae	Tropical	Tropical	0.869	Tropical	0.538 (0.000–0.996)
Fabidae	Tropical	Tropical	0.987	Tropical	0.573 (0.019–0.982)

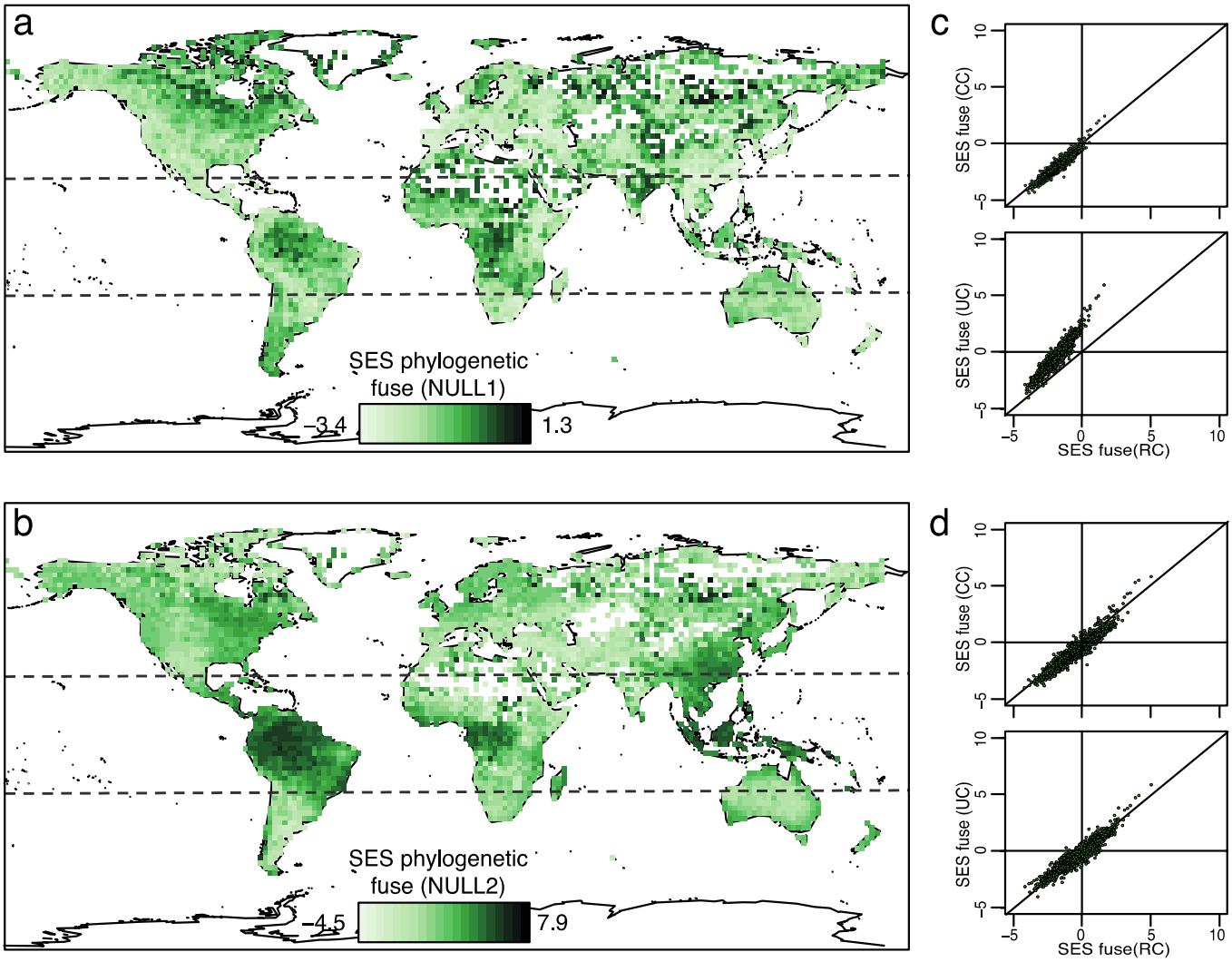

Supplementary Figure 1

Geographic distribution of flowering plant family phylogenetic fuse across the globe based on Bayesian dated phylogenies and geographic occurrence data for all angiosperm families. a-b, standardized effect sizes (SES) for mean family phylogenetic fuses across the globe under the (a) NULL1 and (b) NULL2 spatial models. Estimates based on the dated tree obtained under the relaxed calibration with the complete fossil set. c-d, per grid-cell comparison of standardized effect sizes under the (c) NULL 1 and (d) NULL 2. Negative and positive values indicate grid-cells with shorter and longer mean phylogenetic fuses than expected by chance, respectively (see ***Spatial patterns of Angiosperm diversity*** above).

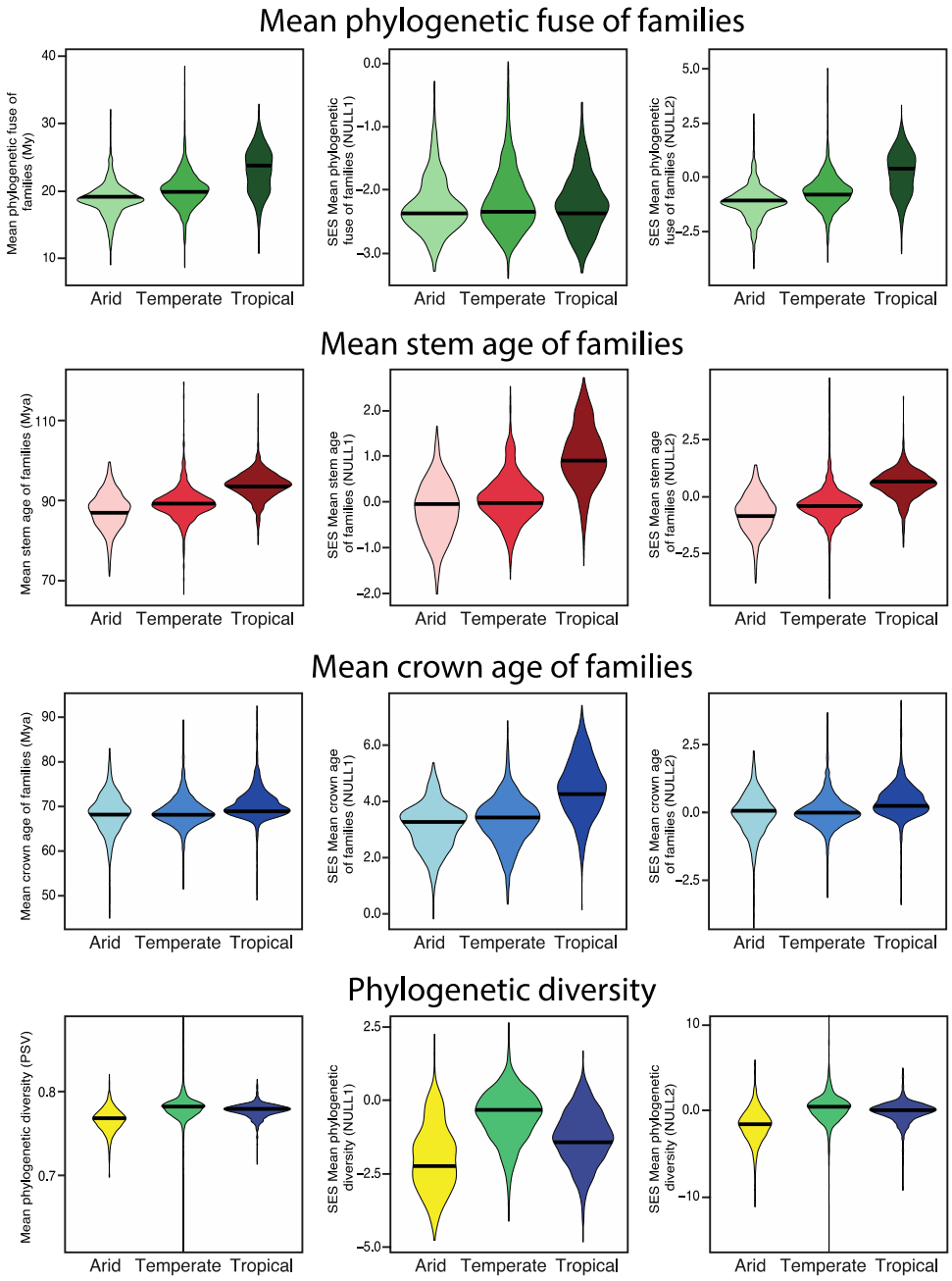

Supplementary Figure 2

Flowering plant family ages and phylogenetic diversity based on a Bayesian dated phylogeny and 16.4 million geographic occurrence records. Probability density (violin plots) for estimated values (left panels) and standardized effect sizes (SES) under the NULL 1 (central panels) and NULL 2 (right panels) across three super biome categories (Arid, Temperate, Tropical) (see ***Spatial patterns of Angiosperm diversity*** above). Solid black lines in violin plots indicate the half range mode of the distributions. Estimates based on the dated tree obtained under the relaxed calibration with the complete fossil set.

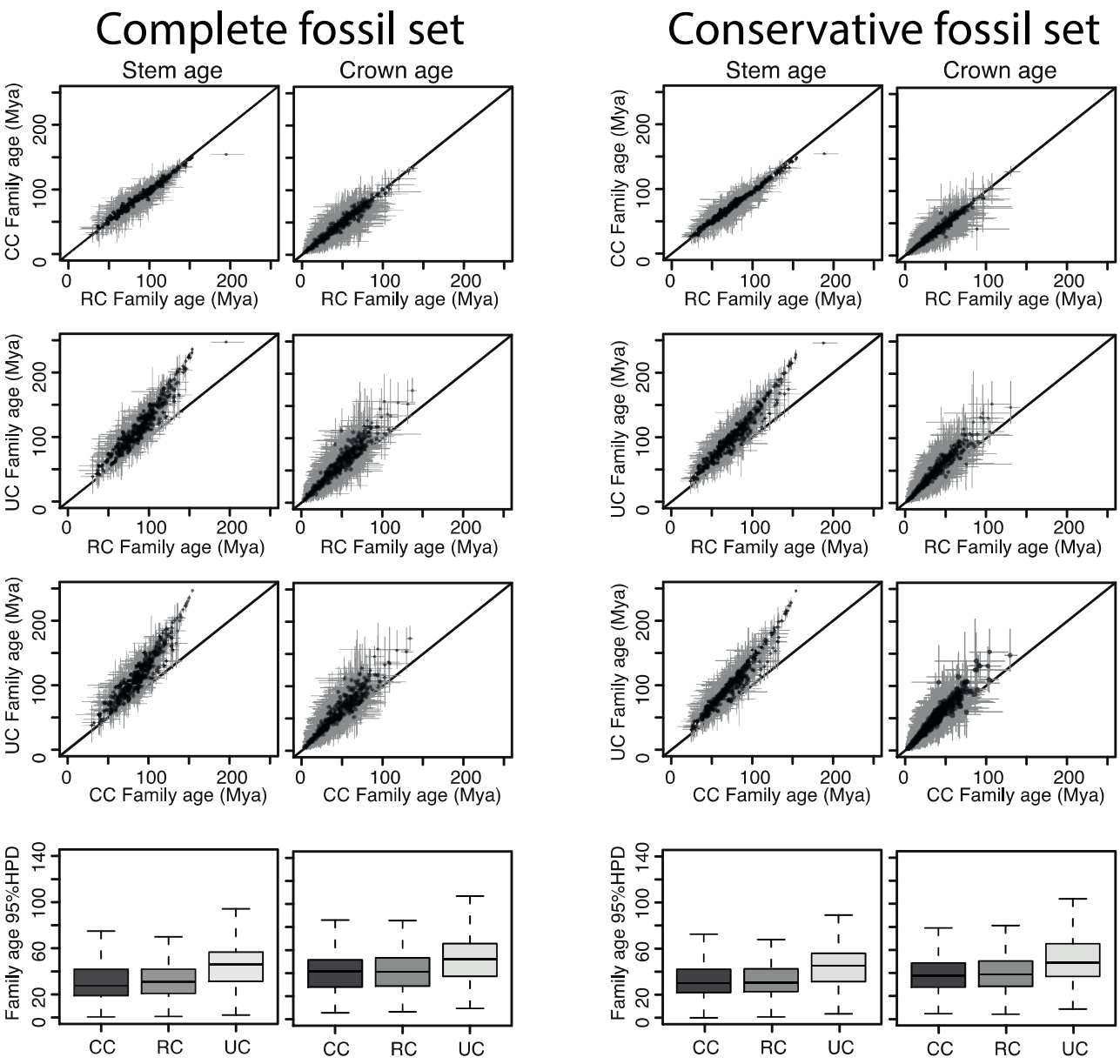

Supplementary Figure 3

Flowering plant family age estimates based on Bayesian dated phylogenies under different calibration strategies. Scatter plots comparing family crown and stem ages between the dating analyses using the complete and the conservative set of fossils for the three calibrations strategies: constrained calibration (CC), relaxed calibration (RC) and unconstrained calibration (UC). Black circles represent mean estimates and grey lines represent the 95% highest posterior density (HPD) intervals. Boxplots showing the distribution of family age 95% highest posterior density (HPD) intervals for the different dating analyses (see ***Family age estimates across analyses*** above).

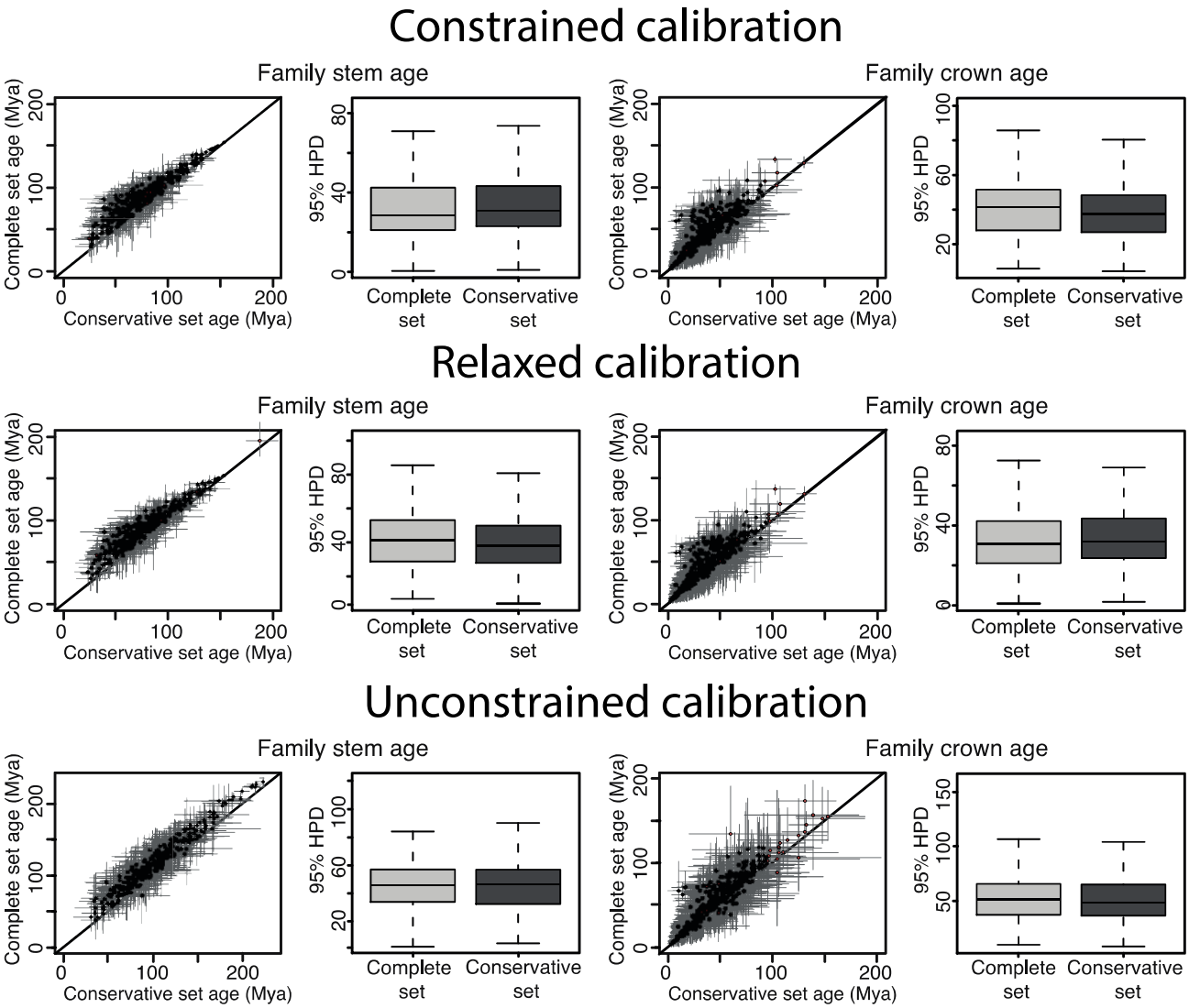

Supplementary Figure 4

Flowering plant family age estimates based on Bayesian dated phylogenies obtained with different fossil calibration sets. Scatter plots comparing family crown and stem ages between analyses using the complete (y-axis) and the conservative set of fossils (x-axis) for the three calibrations strategies. Black circles represent mean estimates and grey lines represent the 95% highest posterior density (HPD) intervals. Boxplots showing the distribution of family age 95% highest posterior density (HPD) intervals for analyses using the complete and conservative set of fossils (see ***Family age estimates across analyses*** above).

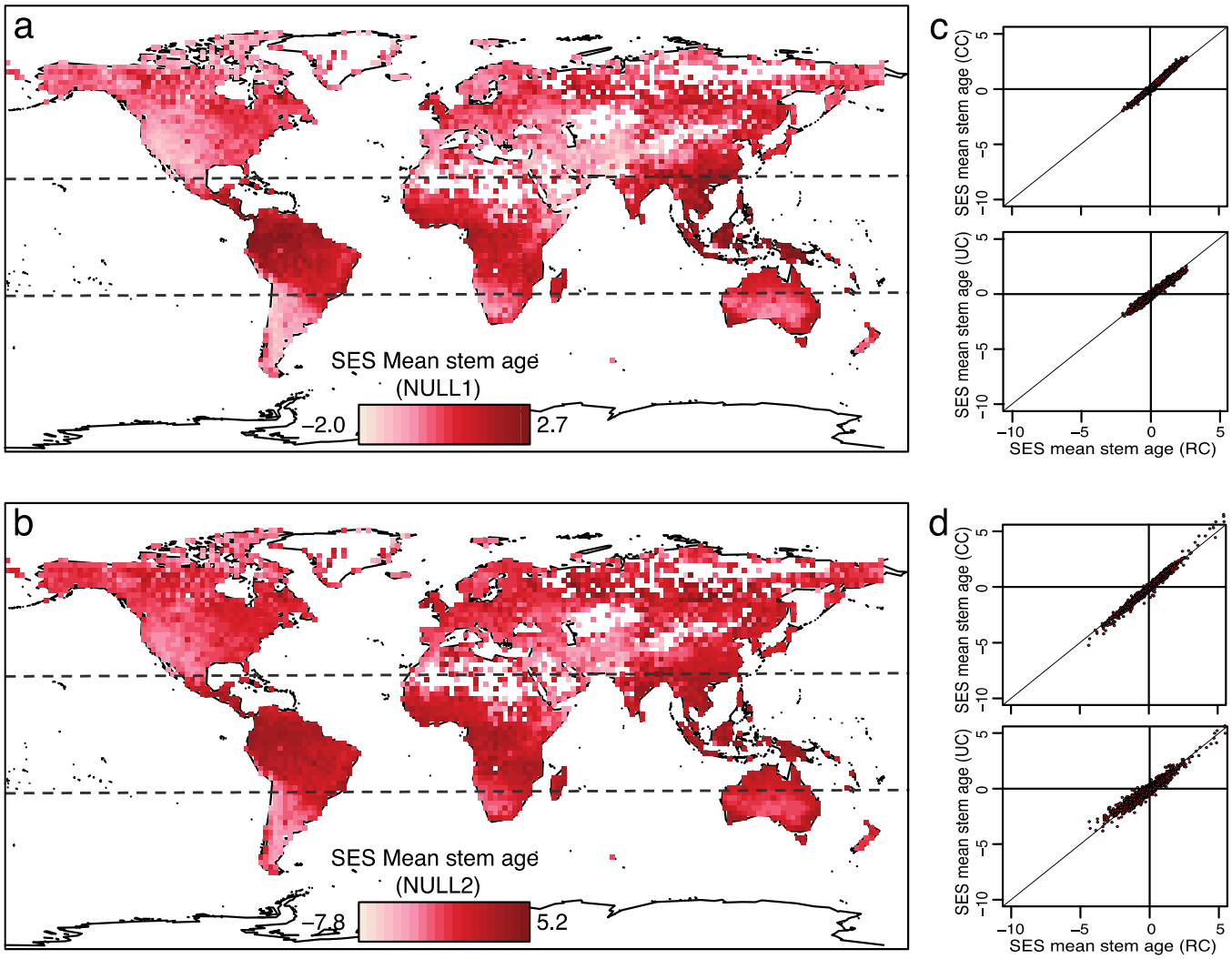

Supplementary Figure 5

Geographic distribution of flowering plant family stem age across the globe based on Bayesian dated phylogenies and geographic occurrence data for all angiosperm families. a-b, standardized effect sizes (SES) for mean family stem age across the globe under the (a) NULL1 and (b) NULL2 spatial models. Estimates based on the dated tree obtained under the relaxed calibration with the complete fossil set. c-d, per grid-cell comparison of standardized effect sizes (SES) under the (c) NULL 1 and (d) NULL 2. Negative and positive values indicate grid-cells with lower and higher mean stem ages than expected by chance, respectively (see ***Spatial patterns of Angiosperm diversity*** above).

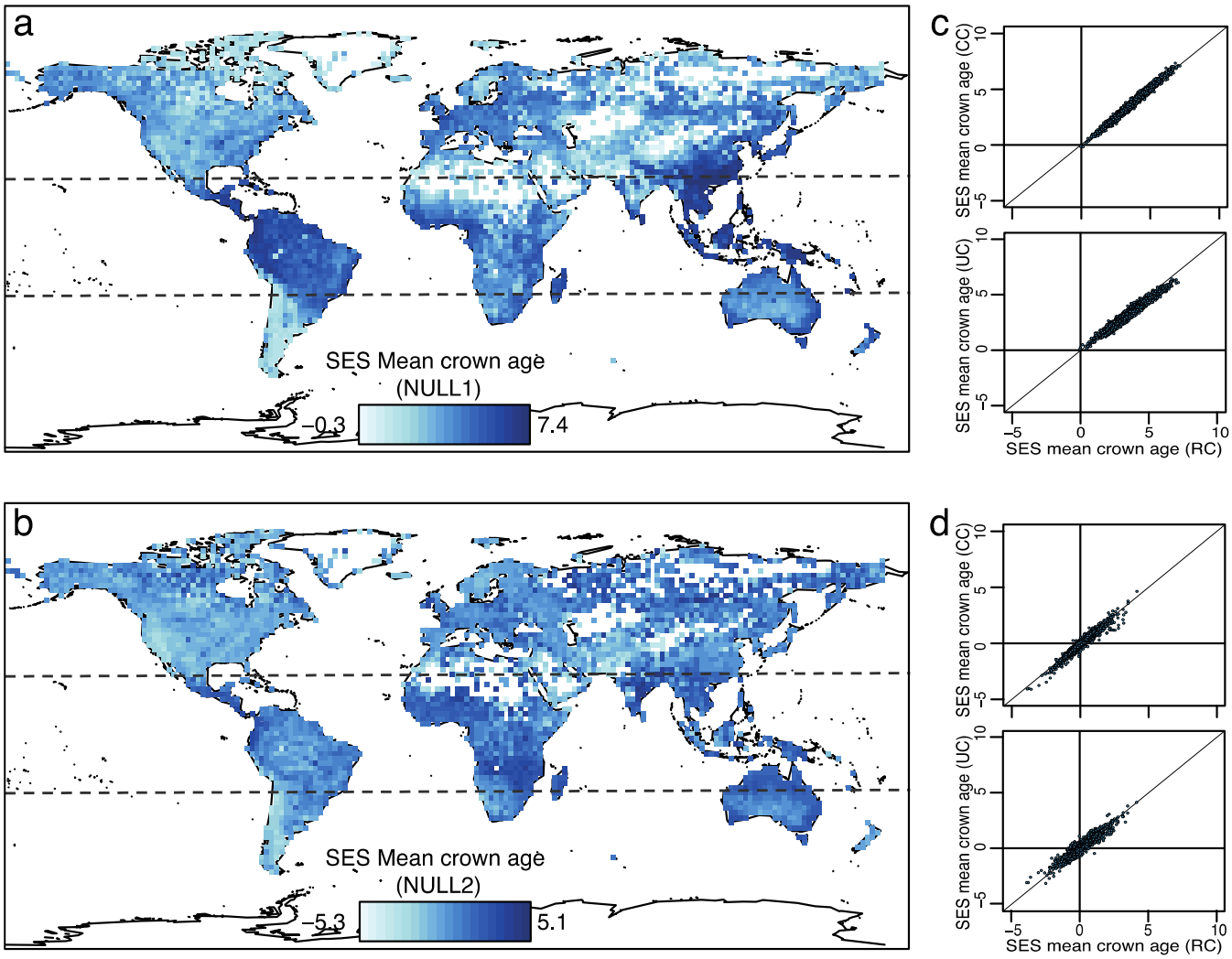

Supplementary Figure 6

Geographic distribution of flowering plant family crown age across the globe based on Bayesian dated phylogenies and geographic occurrence data for all angiosperm families. a-b, standardized effect sizes (SES) for mean family crown age across the globe under the (a) NULL1 and (b) NULL2 spatial models. Estimates based on the dated tree obtained under the relaxed calibration with the complete fossil set. c-d, per grid-cell comparison of standardized effect sizes (SES) under the (c) NULL 1 and (d) NULL 2. Negative and positive values indicate grid-cells with lower and higher mean crown ages than expected by chance, respectively (see ***Spatial patterns of Angiosperm diversity*** above).

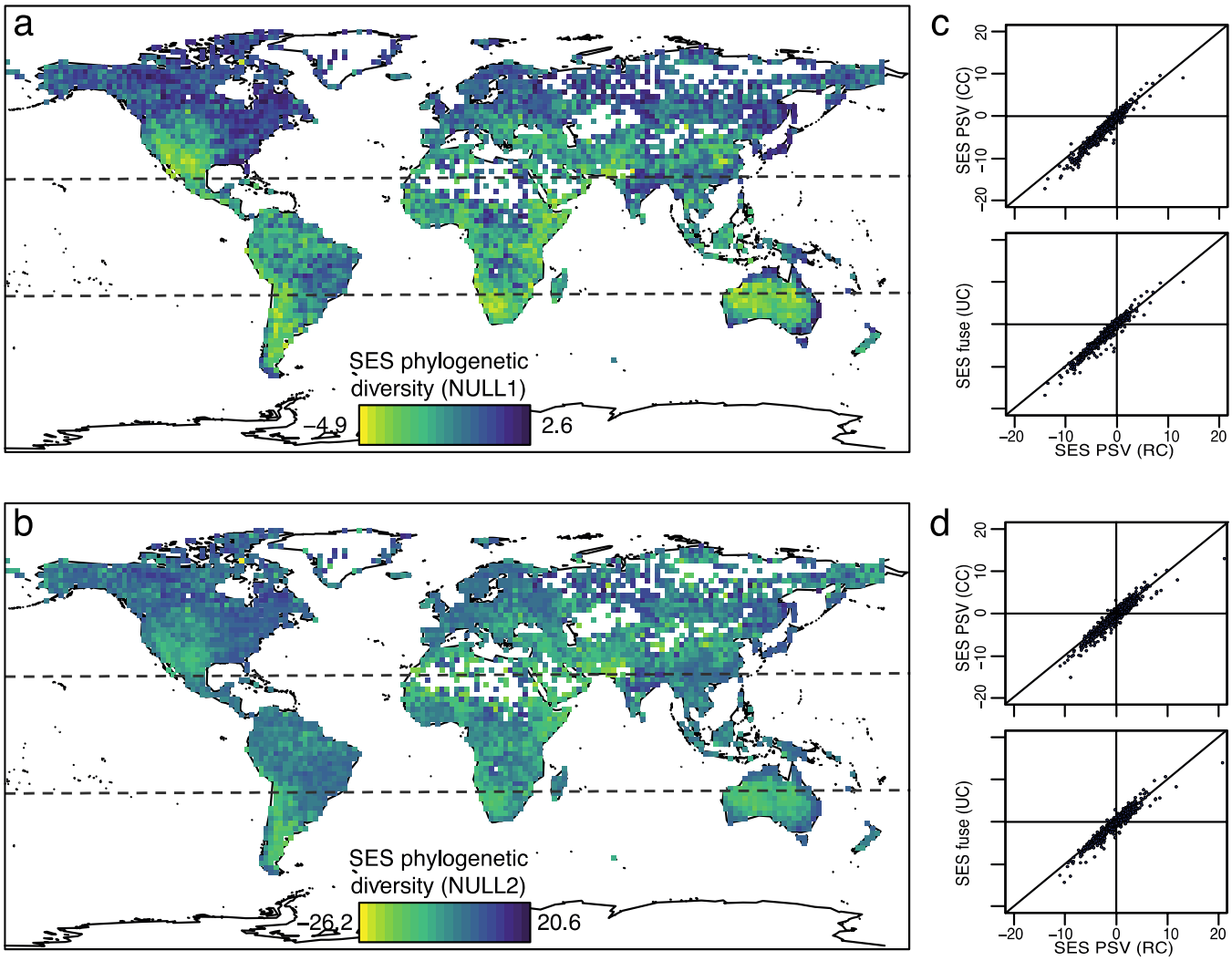

Supplementary Figure 7

Geographic distribution of flowering plant phylogenetic diversity across the globe based on Bayesian dated phylogenies and geographic occurrence data for all angiosperm families. a-b, standardized effect sizes (SES) for the Phylogenetic Species Variability index[55,63] (PSV) across the globe under the (a) NULL1 and (b) NULL2 spatial models. Estimates based on the dated tree obtained under the relaxed calibration with the complete fossil set. c-d, per grid-cell comparison of standardized effect sizes (SES) under the (c) NULL 1 and (d) NULL 2. Negative and positive values indicate grid-cells with lower and higher PSV than expected by chance, respectively (see ***Spatial patterns of Angiosperm diversity*** above).

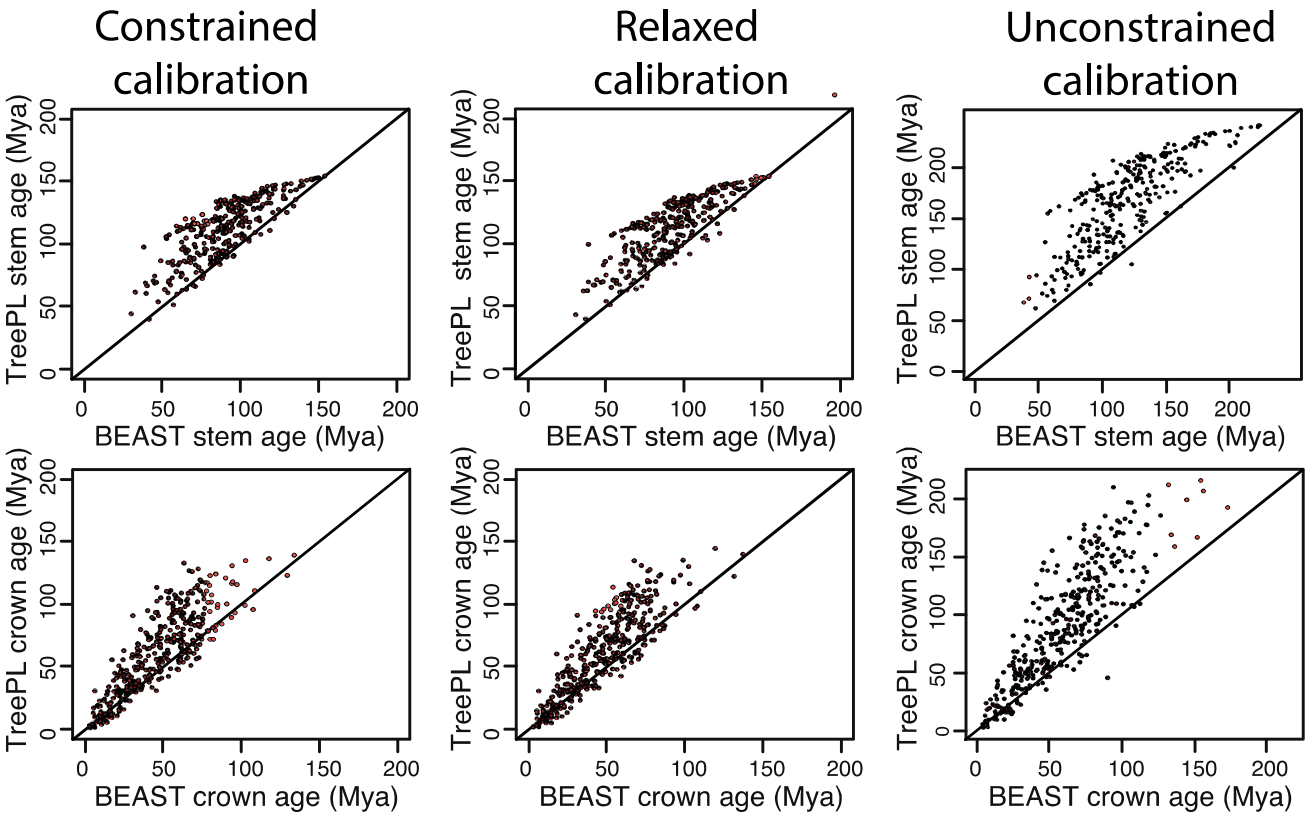

Supplementary Figure 8

Flowering plant family age based on Bayesian and penalized likelihood dated phylogenies under different calibration strategies. Scatter plots comparing family crown and stem ages between Bayesian (BEAST2[44]) and penalized likelihood (treePL[43]) methods under the three analyses differing in maximum age constraints (see ***Family age estimates across analyses*** above).

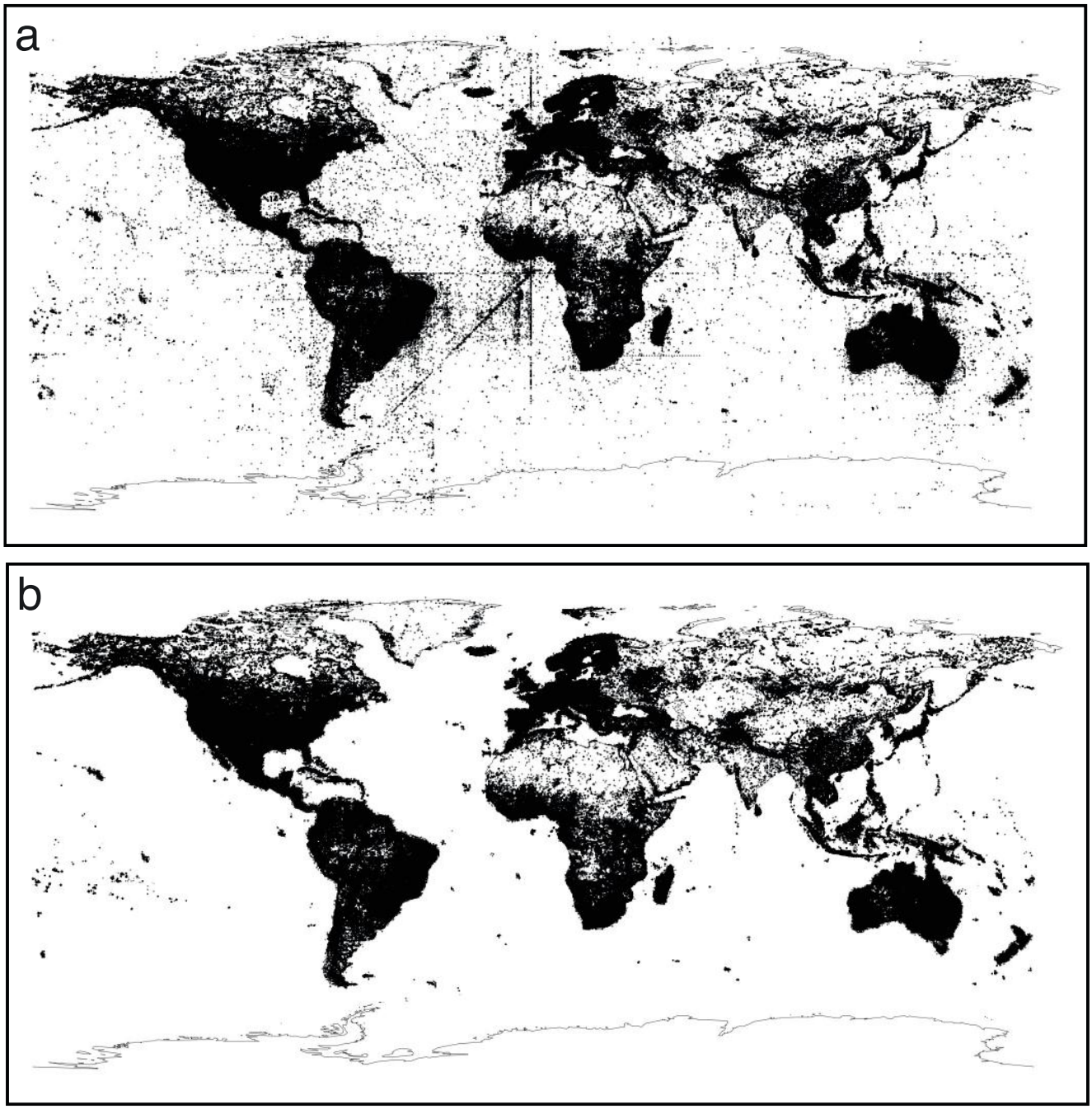

Supplementary Figure 9

Geographical distribution of flowering plant occurrence records across the globe obtained from the Global Biodiversity Information Facility. a, geographic distribution of *c.* 61 million occurrence records for angiosperm species without correction. b, geographic distribution of *c.* 16.4 million occurrence records for angiosperm species after correction (see ***Geographic data processing*** above).

List of Supplementary Data files

- **Data1_ RAxMLTree.tre:** maximum likelihood angiosperm phylogeny (NEWICK format) estimated with RAxML.
- **Data2_PROTEUS (folder):** detail information on the fossils used for calibration provided as a PDF file (Data2a_CalibrationList.pdf) and an Excel worksheet (Data2b_CalibrationList.xlxs).
- **Data3_CalibrationMap.pdf:** angiosperm phylogenetic tree with nodes annotated with the fossils used for calibration (fossil code numbers as in **Data 2**).
- **Data4_ Ages.xlsx:** age for orders, families and subfamilies of angiosperms obtained from the angiosperm dated phylogenies in Data 7.
- **Data5_ AncestralBiomeResults.xlsx:** results of ancestral biome reconstructions for angiosperms using the angiosperm dated phylogenies in **Data 10**.
- **Data6_ AncestralBiomeMap.pdf:** angiosperm phylogenetic tree with nodes annotated with biome reconstructions.
- **Data7_ MolecularDataset.nex:** sequence alignment (NEXUS) used to estimate angiosperm phylogenetic relationships.
- **Data8_MolecularSampling.xlsx:** list of accession numbers for taxa used to estimate angiosperm phylogenetic relationships.
- **Data9_TopologicalConstraints.tre:** topological constraints (NEWICK format) used in the estimation of angiosperm phylogenetic relationships.
- **Data10_BEASTTrees.zip (zipped folder):** angiosperm dated phylogenies estimated under the six calibration schemes in BEAST 2.5.1.